ELSEVIER

International Journal of Mass Spectrometry 204 (2000) 267–280

International Journal of Mass Spectrometry

Structures and fragmentations of zinc(II) complexes of amino acids in the gas phase. II. Decompositions of glycine–Zn(II) complexes

Yannik Hoppilliard, Françoise Rogalewicz*, Gilles Ohanessian

Laboratoire des Mécanismes Réactionnels, DCMR-UMR CNRS 7651, Ecole Polytechnique, 91128 Palaiseau Cedex, France

Received 13 April 2000; accepted 6 June 2000

Abstract

The zinc complex of glycinate $[Gly–H + Zn]^+$ has been formed by electrospray of a glycine/$ZnCl_2$ mixture in a 50:50 vol. water/methanol solution. In this article, the precursors and the fragments of $[Gly–H + Zn]^+$ ions are studied by means of collisional induced decomposition (CID) experiments including H/D exchanges and accurate ab initio calculations. Two precursors were identified: $[Gly + CH_3OH–H + Zn]^+$ (**A**) and $[Gly + Gly–H + Zn]^+$ (**B**), **A** being much more abundant than **B**. The three main fragmentations of $[Gly–H + Zn]^+$ are loss of carbon dioxyde, loss of carbon monoxyde, and successive losses of water and carbon monoxyde. To interpret these fragmentations four structures were chosen to describe $[Gly–H + Zn]^+$. These structures are complexes between Zn(II) and glycine deprotonated either on the carboxylic group $[NH_2CH_2COOZn]^+$ (**1**) or on the amine function $[ZnNHCH_2COOH]^+$ (**2**) or isomeric forms involving ZnH^+ i.e. either $[NH_2CHCOOZnH]^+$ (**3**) or $[HZn \cdots NH{=}CHCOOH]^+$ (**4**) respectively. None of the fragmentations is interpretable directly from structures **1** and **2**. Loss of carbon dioxyde occurs from **3**, loss of carbon monoxyde from a complex **CX** where $HOZn^+$ interacts with CO and $NH{=}CH_2$, a rearranged form of **2**. Successive losses of water and carbon monoxyde can take place from **4**. The non occurrence of structures **1** and **2** during the fragmentation of $[Gly–H + Zn]^+$ ions is interpreted by isomerizations within **A** before evaporation of the last molecule of solvent. These isomerizations are energetically easier than the last step of desolvation. (Int J Mass Spectrom 204 (2000) 267–280) © 2000 Elsevier Science B.V.

Keywords: Electrospray; Desolvation; Mechanisms; Zn(II) complexes; Glycine; CID; *ab initio* calculations

1. Introduction

With the advent of electrospray ionization [1], it has become possible to study dipositively charged transition metal complexes that are prepared as stable or transient species in solution and then transferred to the gas phase. This allows one to study the properties of gas-phase complexes in the absence of solvent, and induce dissociations that provide information on the ligand–metal chemical interactions.

In this series of articles we have focused our interest on the formation and fragmentation of Zn(II)-cationized molecular species formed by electrospray of mixtures of amino acids and $ZnCl_2$ in methanol–water solutions.

The study of metal–amino acid complexes in the gas phase should improve the understanding of the intrinsic binding properties of amino acids to metal ions and highlight characteristic fragmentations al-

* Corresponding author. E-mail: yannik@dcmr.polytechnique.fr

PII S1387-3806(00)00358-4

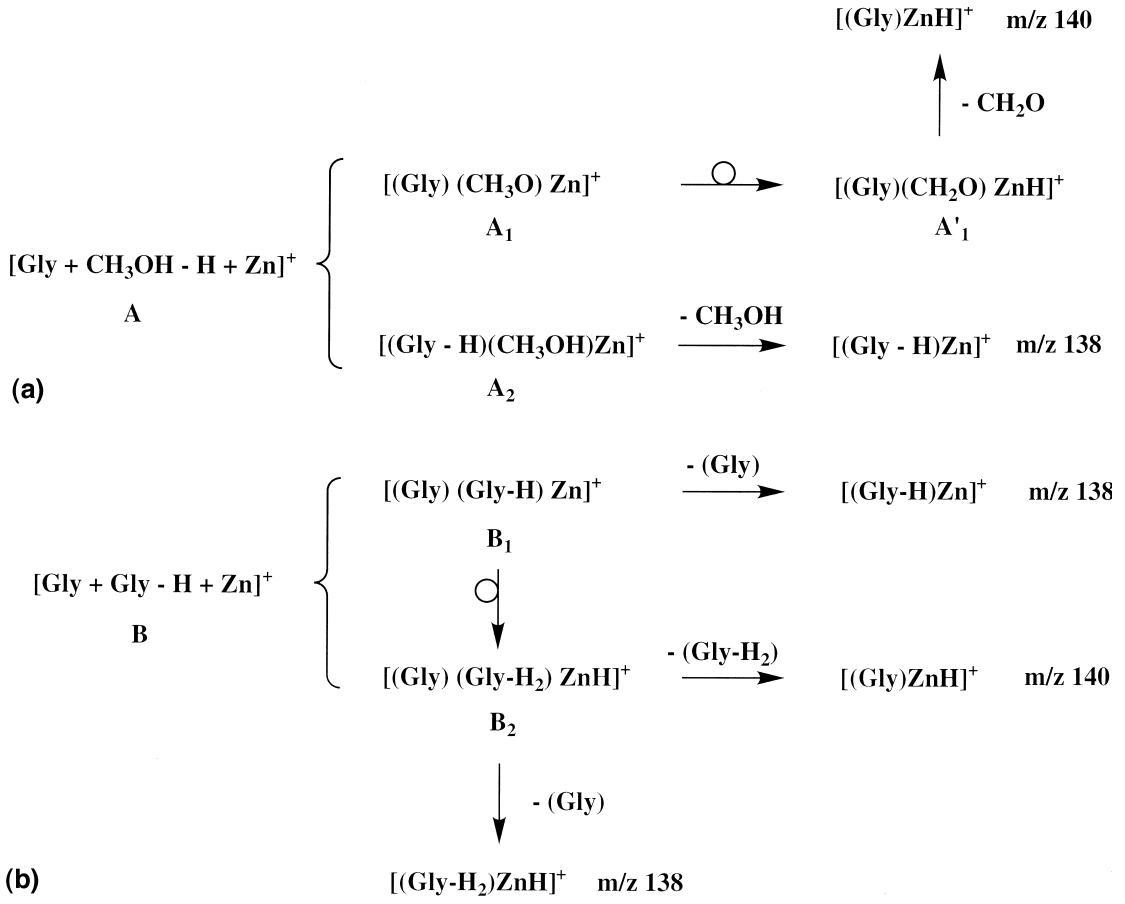

Scheme 1.

lowing the rapid identification of some amino acids in peptides.

In the first article of this series [2], we have shown that the Zn(II)-cationized glycine (Gly) complexes are $[Gly + H + Zn]^+$ (*m/z* 140) and $[Gly–H + Zn]^+$ (*m/z* 138). These ions have two common precursors identified as $[Gly + CH_3OH–H + Zn]^+$ (**A**) and $[Gly + Gly–H + Zn]^+$ (**B**) (Scheme 1). The hydrogen eliminated was demonstrated to be an exchangeable hydrogen by H/D exchange experiments. The main conclusion of this article was that the formation of molecular ions may involve rearrangements of their precursors.

In the solvated precursor, **A**, the deprotonated species may be either the solvent molecule: $[(Gly)(CH_3O)Zn]^+$ ($\mathbf{A_1}$) or the sample molecule: $[(Gly–H)(CH_3OH)Zn]^+$ ($\mathbf{A_2}$) [Scheme 1(a)]. Ab initio calculations show that $\mathbf{A_1}$ and $\mathbf{A_2}$ are very close together in energy. Direct loss of methanol from $\mathbf{A_2}$ to give $[Gly–H + Zn]^+$ is calculated to be more energy demanding than rearrangement of $\mathbf{A_1}$ into $[(Gly)(CH_2O)ZnH]^+$ ($\mathbf{A_1'}$) followed by elimination of CH_2O to give $[Gly + H + Zn]^+$ [Scheme 1(a)]. This result is in agreement with collisionally induced decomposition (CID) experiments. In the CID spectra of **A**, $[Gly + H + Zn]^+$ appears at lower collision energy than $[Gly–H + Zn]^+$.

The deprotonated dimer $[Gly + Gly–H + Zn]^+$ (**B**) may also exist in two different forms: $[(Gly)(Gly–H)Zn]^+$ noted $\mathbf{B_1}$ and $[(Gly)(Gly–H_2)ZnH]^+$ noted $\mathbf{B_2}$. Direct elimination of Gly from $\mathbf{B_1}$ leads to $[(Gly–H) + Zn]^+$ [Scheme 1(b)]. However, formation of $[Gly + H + Zn]^+$ from $[(Gly)(Gly–H)Zn]^+$ ($\mathbf{B_1}$) requires a rearrangement into $[(Gly)(Gly–H_2)ZnH]^+$

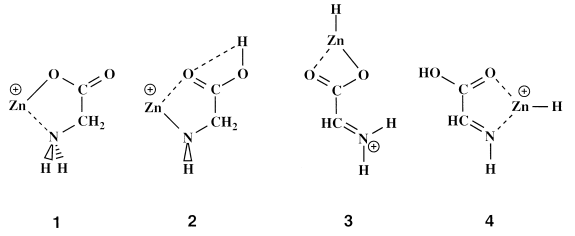

Scheme 2.

(**B_2**). The deuteration experiments show that the hydrogen atom involved in the rearrangement is one of the $–CH_2–$ group. Competitive eliminations of Gly or (Gly–H_2) from the rearranged structure (**B_2**) lead to $[Gly + H + Zn]^+$ with structure $[(Gly)ZnH]^+$ and to $[Gly–H + Zn]^+$ with structure $[(Gly–H_2)ZnH]^+$.

Nine structures were chosen [2] to represent the $[Gly–H + Zn]^+$ ion. Their relative stabilities were evaluated by accurate ab initio calculations. Among these structures the four most stable (**1–4**, Scheme 2) were retained to represent the $[Gly–H + Zn]^+$ ion in the present work.

All of them are consistent with the loss of a labile hydrogen during the formation of $[Gly–H + Zn]^+$. Structures **1** and **2** result from direct deprotonation of either the carboxylic or the amine function, respectively. Structures **3** and **4** are rearranged forms of **1** and **2**, respectively, through β-H transfer from C to Zn.

Are the low energy fragmentations of $[Gly–H + Zn]^+$ interpretable from these structures? Or do we need to invoke rearrangements of these structures, or even rearrangements within their incompletely desolvated precursors, to interpret these fragmentations? The goal of this paper is to answer these questions. The precursors and fragment ions of $[Gly–H + Zn]^+$ and of its fragment ions were studied by CID experiments in a triple quadrupole mass spectrometer. The energies associated with the various fragmentation reactions were evaluated by means of ab initio calculations.

2. Experimental and theoretical procedures

2.1. Experimental

Electrosprayed zinc complexes of methanol and glycine were formed from a glycine/$ZnCl_2$ mixture (500 and 250 μM, respectively) in a 50:50 vol. water/methanol solution. Such concentrations are typical for the formation of metal complexes of amino acids. In such conditions, the pH is in the 6.5–7 range. Labeling experiments were performed by H/D exchanging all exchangeable hydrogens of glycine in a D_2O/CH_3OD solution. Solutions were infused in the ion source with a syringe pump (Harvard, Southnatic, MA, USA) at a flow rate of 10 μL/mn. L-Gly was purchased from Aldrich Chem. Co. (Saint Quentin Fallavier, France) and anhydrous $ZnCl_2$ was obtained from Merck KGaA (Darmstadt, Germany). All solvents were of HPLC grade.

All experiments were carried out on a triple quadrupole Quattro II mass spectrometer (Micromass, Manchester, UK). Source parameters were adjusted so as to optimize ion signals (such as $[Gly–H + Zn]^+$). Typical voltage values were: capillary 2.5–3.5 kV, counter electrode 0.1–0.3 kV, rf lens 0.7 eV, skimmer 1.5 V. Source spectra were recorded with a sampling cone voltage of 40 V.

Low energy CID of $[Gly–H + Zn]^+$ and its fragments were performed with argon as the collision gas. The decomposition of $[Gly–H + Zn]^+$ was studied as a function of collision energy in the laboratory frame (E_{lab}). The breakdown graph associated with the abundances of the various fragment ions as a function of collision energy, is given in Fig. 1.

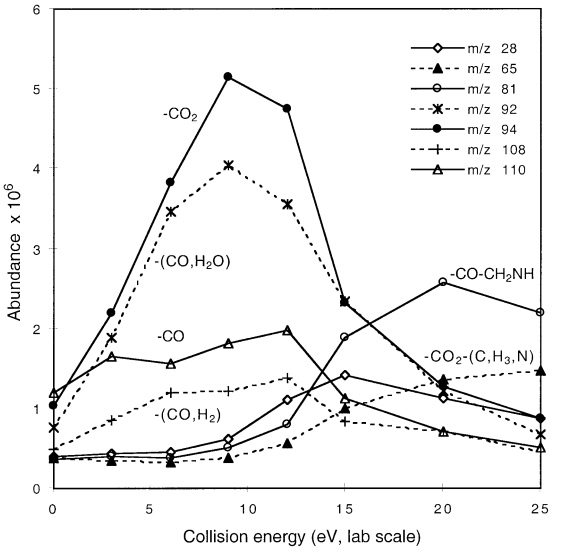

Fig. 1. Breakdown graph of $[Gly–H + Zn]^+$ (*m/z* 138) (sampling cone voltage = 40 V).

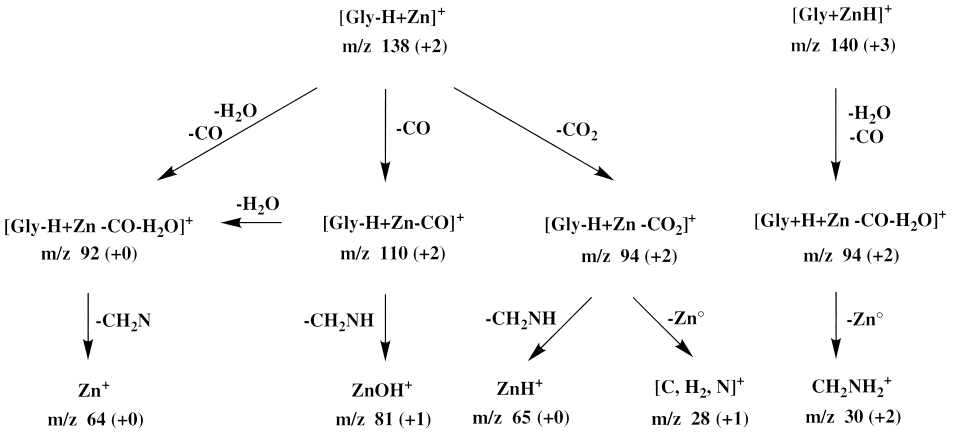

Scheme 3.

Parent ion scans of all fragment ions observed in the breakdown graph were recorded in the following conditions: the collision energy in the laboratory frame was set to 12 eV and the collision gas pressure was adjusted so as to diminish the parent ion intensity by 50%–70%; before each experiment, the resolution of the first quadrupole and the extraction cone voltage were set to maximize the intensity of the parent ion. This led to a cone voltage of 40 V and a collision gas pressure of $\sim 10^{-3}$ mbar. Fragment ion scans of the most abundant fragment ions (*m/z* 110, 94, and 92) were recorded at higher cone voltages and for collision energies close to 10 eV.

2.2. Computational

Two basis sets were used in this study. For geometry optimizations and vibrational frequency calculations, the 6-31G* basis was used for H, C, N, and O, and the polarized Wachters [14*s*9*p*5*d*1*f*/9*s*5*p*3*d*1*f*] was used for Zn [3]. This is referred to as basis1. For final energy calculations, basis2 consists in the 6-311 + G(2*d*,2*p*) for H, C, N, and O, and the extended Wachters basis [15*s*11*p*6*d*2*f*/10*s*7*p*4*d*2*f*] for Zn [3]. Geometry optimizations and vibrational frequency calculations were generally carried out at the second order Møller-Plesset (MP2)(FC)/basis 1 level (where FC means that the frozen core approximation was used), but for methanol solvated complexes, the Hartree-Fock (HF) level was used. Extensive tests described in reference 2 showed that the use of HF geometries leads to very small errors in final energy calculations. Final energetics were obtained with MP2(FC)/basis2 wave functions at the MP2(FC)/basis1 or HF/basis1 geometries. These levels are denoted below as MP2/basis2//MP2/basis1 and MP2/basis2//HF/basis1, respectively. The GAUSSIAN94 program package [4] was used throughout.

3. Results

3.1. Fragmentations of $[Gly–H + Zn]^+$ induced by low energy collisions

The fragment ions generated by collisional activation of $[Gly–H + Zn]^+$ (*m/z* 138) are shown in Fig. 1 as a function of collision energy. Zinc containing ions are characterized by multiple peaks due to the naturally occurring zinc isotopes of *m/z* 64, 66, 67, 68, and 70 with natural relative abundances of 48.89%, 27.81%, 4.11%, 18.56%, and 0.62%, respectively. In what follows, we will always mention the mass of a zinc containing ion with reference to the smallest mass-to-charge ratio, which corresponds to the most abundant zinc isotope (*m/z* = 64).

At low collision energies ($E_{lab} < 5$ eV), four ions of significant abundance are observed in the CID spectrum: the molecular ion, $[Gly–H + Zn]^+$ at *m/z* 138 and three fragment ions at *m/z* 110 (loss of 28 u),

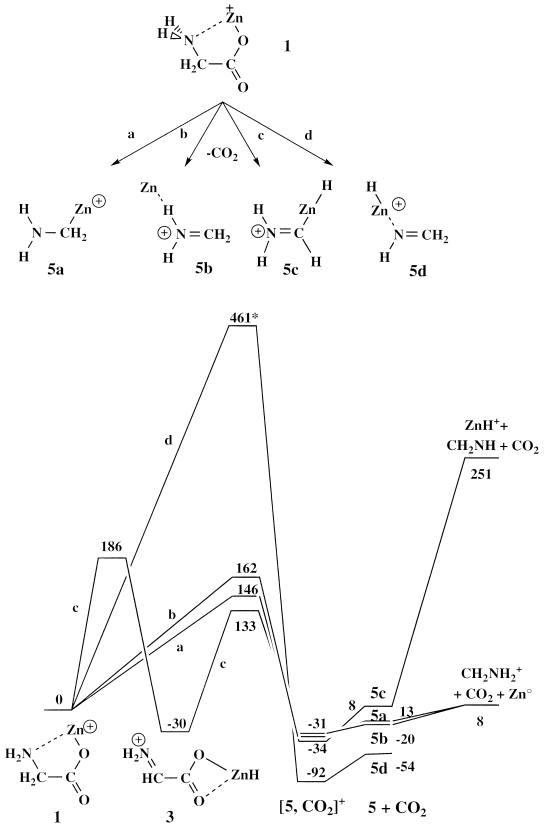

Fig. 2. Potential energy profiles associated with decarboxylation of **1** and **3**.

m/z 94 (loss of 44 u), and *m/z* 92 (loss of 46 u). After H/D exchange of labile hydrogens in $[Gly–H + Zn]^+$, these ions are shifted to *m/z* 140 (+2), 112 (+2), 96 (+2), and 92 (+0). The fragment ions are identified as $[Gly–H + Zn–CO]^+$, $[Gly–H + Zn–CO_2]^+$, and $[Gly–H + Zn–H_2O–CO]^+$, respectively. In the latter, both hydrogen atoms eliminated in the water molecule are labile hydrogens.

At higher collision energies ($E_{lab} > 5$ eV), other fragment ions are observed at *m/z* 81 (loss of 57 u), *m/z* 65 (loss of 73 u), and *m/z* 28 (loss of 110 u). After H/D exchange of the labile hydrogens in the molecular ion, these fragment ions appear at *m/z* 82 (+1), 65 (+0), and 29 (+1) and are identified as $[ZnOH]^+$, $[ZnH]^+$, and $[C, H_2, N]^+$, respectively.

Precursor and fragment ion spectra of *m/z* 110, 94 and 92, formed in the source were recorded for V_c = 40 V and E_{lab} = 12 eV. The reaction diagram associated with the formation and decomposition of these ions is given in Scheme 3.

The unique parent ion of *m/z* 110 is $[Gly–H + Zn]^+$. The CID spectrum of this $[Gly–H + Zn–CO]^+$ ion shows two fragment ions at *m/z* 92 (loss of H_2O) and *m/z* 81 (loss of CH_2NH).

Parent ion scans show both $[Gly + H + Zn]^+$ and $[Gly–H + Zn]^+$ as precursors for *m/z* 94. After H/D exchange in the precursors, *m/z* 94 is totally shifted to *m/z* 96 in agreement with loss of CO_2 from $[Gly–H + Zn]^+$ and of (H_2O + CO) from $[Gly + H + Zn]^+$, the water molecule including one labile hydrogen only. CID of *m/z* 94 ions leads to *m/z* 65, *m/z* 30, and *m/z* 28 identified respectively as $[ZnH]^+$, the immonium ion $[CH_2–NH_2]^+$ and an ion of general formula $[C, H_2, N]^+$. Since *m/z* 30 does not appear in the breakdown graph of $[Gly–H + Zn]^+$ (Fig. 1), this ion is expected to be exclusively formed from $[Gly + H + Zn–H_2O–CO]^+$ by loss of Zn °. This hypothesis is confirmed, at high collision energy, by the presence in the CID spectrum of $[Gly + H + Zn]^+$ of the *m/z* 30 ion whereas *m/z* 65 and 28 are not observed. The *m/z* 94 ions formed in the source are therefore a mixture of two ions: $[Gly–H + Zn–CO_2]^+$ and $[Gly + H + Zn–H_2O–CO]^+$, having different fragmentation patterns and consequently different structures.

Parent ion scans also reveal two precursors for the *m/z* 92 ion: $[Gly–H + Zn]^+$ and $[Gly–H + Zn–CO]^+$. As *m/z* 92 remains unshifted after H/D exchange in the precursors, the formation of this ion is attributed to a loss of H_2O and CO from $[Gly–H + Zn]^+$ and of H_2O from $[Gly–H + Zn–CO]^+$. Moreover, in the breakdown graph on Fig. 1, the increase in abundance of the *m/z* 92 ion is not associated with a decrease of the $[Gly–H + Zn–CO]^+$ ion. This is only compatible with two competitive mechanisms leading to the formation of *m/z* 92. CID of *m/z* 92 ions formed from either precursor leads to Zn^+ at *m/z* 64.

3.2. Fragmentation mechanisms of $[Gly–H + Zn]^+$

The three primary fragmentations of $[Gly–H + Zn]^+$ are loss of carbon dioxyde, loss of carbon

monoxyde and successive losses of water and carbon monoxyde.

The initial, transition, intermediate and final states associated with these fragmentations were calculated at various levels of theory as given in Tables 1–4. However, in the text relative energies are only given at the highest level of theory which is MP2/basis2//MP2/basis1, taking the total energy of **1** as the reference.

The mechanisms for each of the three fragmentations observed will now be described in turn.

3.3. Loss of CO_2 from structure 1

Among the four structures of $[Gly–H + Zn]^+$ (**1–4**, Scheme 2), the species cationized on the carboxylate and amino functions (structure **1**) seems the most adequate precursor for loss of CO_2 since it only requires breaking of the C–C bond to yield CO_2 and a zincated immonium ion. This may lead to either of two isomeric complexes: $[H_2N–H_2C{-}{-}Zn]^+$ **5a** or $[CH_2–HNH{-}{-}Zn]^+$ **5b** (see Fig. 2). Each mechanism involves two steps: rearrangement of **1** into a complex between CO_2 and either **5a** or **5b**; decoordination of CO_2 from the reaction intermediates [**5a**, CO_2] and [**5b**, CO_2]. The potential energy profiles associated with these reactions are given in Fig. 2. The transition states associated with the first step are located 146 and 162 kJ/mol higher in energy than **1** for **TS 1–**[**5a**, CO_2] and **TS 1–**[**5b**, CO_2], respectively. The intermediate complexes are very close together in energy and more stable than **1** (−34 and −32 kJ/mol for [**5a**, CO_2] and [**5b**, CO_2] respectively, see Table 1). Since the last step consists in a simple bond cleavage, there is no transition state and the critical energy is that of the final state (−13 and −20 kJ/mol for **5a** + CO_2 and **5b** + CO_2, respectively). The rate determining step of decarboxylation leading to either **5a** or **5b** is the elongation of the C–C bond. However, **5a** and **5b** only require 21 and 28 kJ/mol, respectively, to fragment into the immonium ion and the reduced metal Zn °, a new final state ($[NH_2CH_2]^+$ + Zn ° + CO_2) located only 8 kJ/mol above **1**. As the immonium ion is never observed in the CID spectra of $[Gly–H + Zn]^+$, we conclude that decarboxylation does not occur from **1** by way of the intermediates [**5a**, CO_2] and [**5b**, CO_2].

Table 1
Relative energies (in kJ/mol) associated with the various extrema describing the decarboxylation of **1** at various levels of theory

	HF/basis1	MP2/basis1	MP2/basis2//MP2/basis1
1	0	0	0
TS 1–3	219	213	186
3	−49	−48	−30
TS 1–[**5a**, CO_2]	174	139	146
TS 1–[**5b**, CO_2]	242	158	162
TS 3–[**5c**, CO_2]	116	124	133
TS 1–[**5d**, CO_2]	461	—	—
[**5a**, CO_2]	—	−55	−34
[**5b**, CO_2]	—	−25	−32
[**5c**, CO_2]	−54	−48	−31
[**5d**, CO_2]	—	−118	−92
5a + CO_2	—	−23	−13
5b + CO_2	−68	−16	−20
5c + CO_2	−18	−7	8
5d + CO_2	−90	−81	−54

As the CID spectra of $[Gly–H + Zn–CO_2]^+$ exhibit a fragment ion at *m/z* 65 corresponding to ZnH^+, it may be expected that it arises from a rearranged form of **1** involving a ZnH species. The hydrogen transferred on the metal originates either from the carbon or from the nitrogen atom. Since *m/z* 65 is not shifted at all after H/D exchange of the labile hydrogens in $[Gly–H + Zn]^+$, the rearrangement must involve the migration of a nonlabile hydrogen from the carbon atom. Hydrogen transfer from CH_2 to Zn leads to **3** (Scheme 2). The rearrangement of **1** into **3** by way of the transition state **TS 1–3** was described earlier (see [2]). The relative energies associated with **TS 1–3** and **3** are 186 and −30 kJ/mol, respectively. Decarboxylation of **3** leading to [**5c**, CO_2] occurs through a transition state, **TS 3–**[**5c**, CO_2], located 53 kJ/mol below **TS 1–3** (Fig. 2). The intermediate complex is very stable (−31 kJ/mol below **1**) and loses easily CO_2 to give **5c**. The energy required for this dissociation is low: 39 kJ/mol. Further decomposition of **5c** into ZnH^+ and $H_2C{=}NH$ is highly

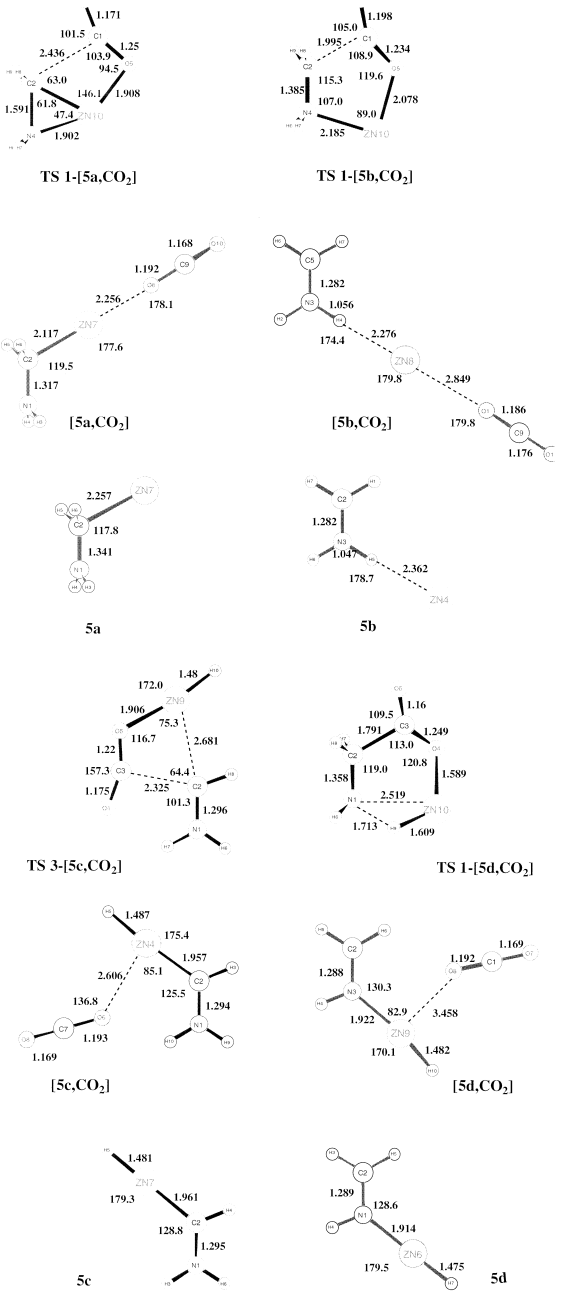

Fig. 3. Decarboxylation of **1** and **3**: Geometries calculated at the MP2/basis1 level. (a) Geometries of **TS 1–[5a**, CO_2]; [**5a**, CO_2]; **5a** and of **TS 1–[5b**, CO_2]; [**5b**, CO_2]; **5b**. (b) Geometries of **TS 3–[5c**, CO_2] and [**5c**, CO_2]; **5c** and of **TS 1–[5d**, CO_2]; and [**5d**, CO_2]; **5d**.

demanding (243 kJ/mol), explaining the appearance of *m/z* 65 only at high collision energy.

The lack of migration of amino hydrogens in the rearrangement of **1** into **3** is confirmed by the potential energy profile of Fig. 2. The very high activation energy required for inserting Zn into a N–H bond (461 kJ/mol at the HF/basis1 level) prevents the formation of the [**5d**, CO_2] complex in agreement with experimental results.

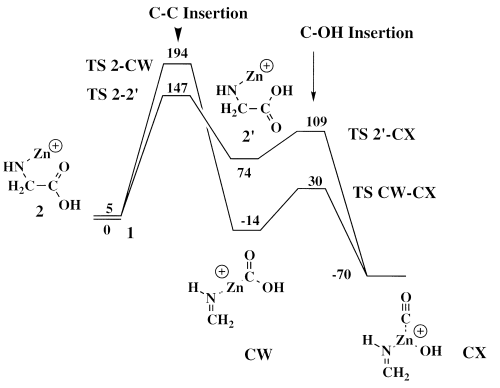

Fig. 4. Potential energy profile associated with isomerization of **2** into the **CX** complex. The energy of **1** is taken as the reference.

The relative energies of the various species describing the decarboxylation of **1** are given in Table 1. The geometries of transition, intermediate and final states, calculated at the MP2/basis1 level, are shown in Fig. 3(a) and (b), respectively.

In summary, the decarboxylation of [Gly–H + Zn]$^+$ cannot take place from zinc glycinate (**1**) since it would necessarily be accompanied by loss of Zn °, a process which is not observed. It must therefore start from an isomeric structure [NH_2=CH–COO–Zn–H]$^+$ (**3**). Since decarboxylation of **1** is calculated to require less energy than that of **3**, we are led to the conclusion that isomer **1**, although the most appealing at first sight, is never formed in the gas phase. The formation of **3** has been discussed previously [2].

*3.4. Loss of CO and of CO and H_2O from structure **2***

The breakdown graph of Fig. 1 shows decarbonylation to be the easiest fragmentation at very low collision energy. This loss of CO is followed by a loss of CH_2NH or of H_2O. The latter includes two labile hydrogens (vide supra). Taking this into account,

Table 2
Relative energies (in kJ/mol) associated with the various extrema describing the isomerization of **2** into the three-ligand complex **CX**, at various levels of theory

	HF/basis1	MP2/basis1	MP2/basis2// MP2/basis1
1	0	0	0
2	42	10	5
TS 1–CW	170	192	194
CW	...	−51	−14
TS CW–CX	46	31	30
TS 2–2′	164	162	147
2′	92	90	74
TS 2′–CX	164	154	109
CX	−72	−51	−70

these consecutive fragmentations require an initial structure of $[Gly–H + Zn]^+$ which is deprotonated on nitrogen. Thus **2** (Scheme 2) is proposed as the precursor for loss of CO. It is only 5 kJ/mol higher in energy than **1**.

The decarbonylation from structure **2** involves the breaking of both the C–C and the C–OH bonds. Two mechanisms are proposed to describe the rearrangement of **2** into a complex $[CH_2NH, ZnOH, CO]^+$, **CX**, a very stable three-ligand species (−70 kJ/mol below **1**), able to eliminate CO as the weakest binding ligand (see Fig. 4).

The first mechanism (1) starts with metal insertion into the C–C bond and leads to the complex $[CH_2NH, ZnCOOH]^+$ (**CW**). A second insertion, into the C–OH bond, gives rise to **CX**. The second mechanism (2) requires a rotation (180 °) of the carboxylic function around the C–C bond, followed by metal insertion into the C–OH bond, which is likely to be accompanied by the cleavage of the C–C bond. The potential energy profiles of both rearrangements are given in Fig. 4, the relative energies of initial, transition, intermediate and final states are gathered in

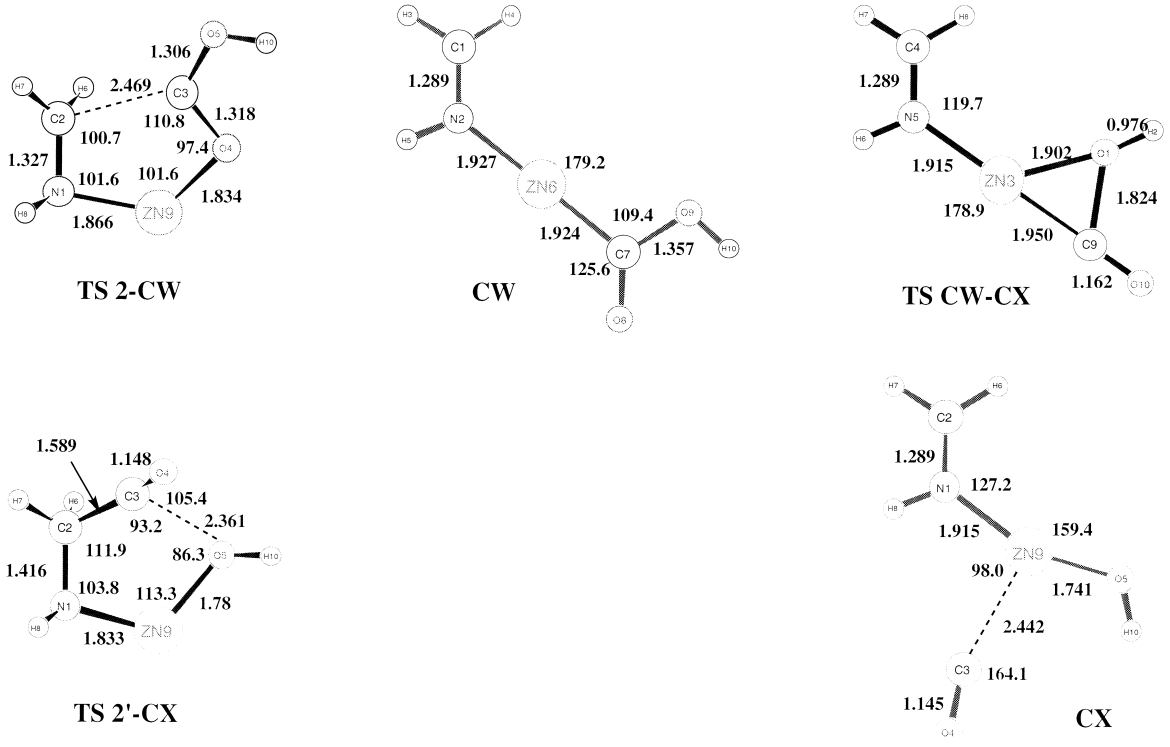

Fig. 5. Isomerization of **2** into **CX**: geometries of **CW**, **CX**, **TS 2–CW**, **TS CW–CX**, **TS 2′–CX**, calculated at the MP2/basis1 level.

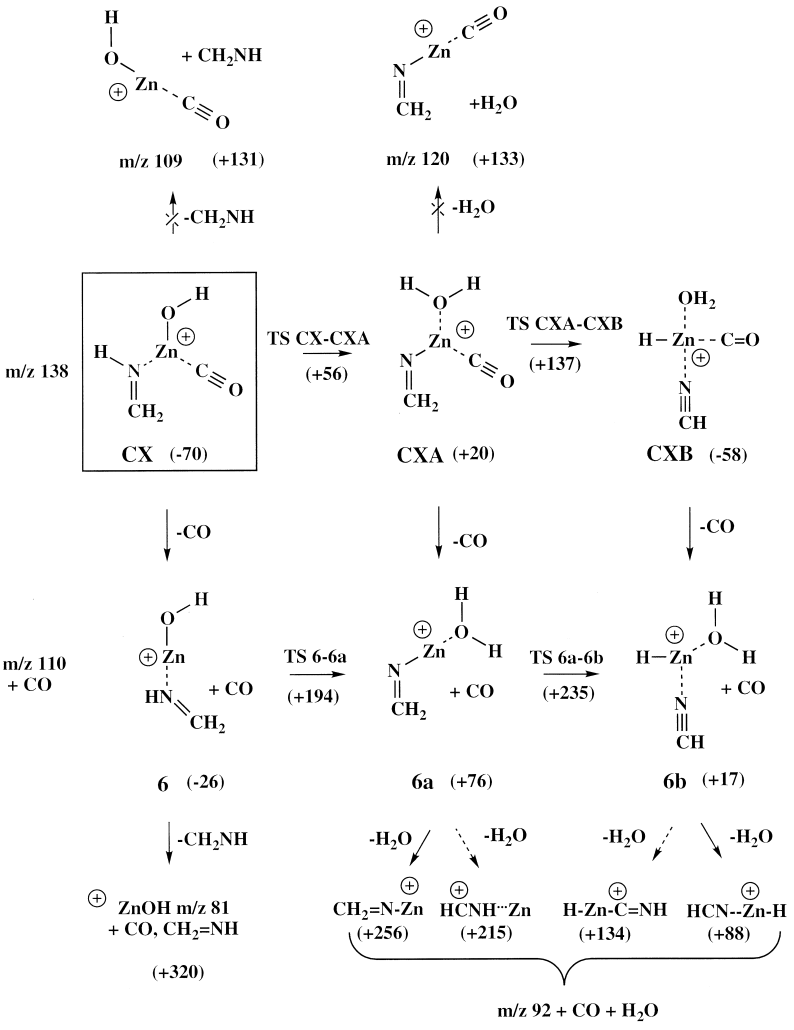

Scheme 4.

Table 2, and the corresponding optimized structures are shown in Fig. 5. The rate limiting step of mechanism (1) is the insertion into the C–C bond with a transition state **TS 2–CW** located 194 kJ/mol above **1**, i.e 189 kJ/mol above **2**. The rate determining step for mechanism (2) is the rotation of the COOH group around the C–C bond leading to **2′**. The energy barrier associated with the change of conformation is calculated to be 142 kJ/mol higher than **2**. Comparison of critical energies shows that mechanism (2) is energetically favoured. The geometries of minima and transition states associated with the transformation of **2** into **CX** are given in Fig. 5.

Two neutral species: CO and CH_2NH, are in interaction with $HOZn^+$ in the three-ligand complex **CX**. Loss of either CO or CH_2NH leads to a final state which is located below **TS 2–2′** (−26, 131, and 147 kJ/mol, respectively). Therefore both processes could occur competitively and spontaneously from **CX**. However, the final state $[HOZn \cdots CO]^+ + CH_2NH$ being much higher in energy (+131 kJ/mol) than $[HOZn \cdots CH_2NH]^+$ (**6**) + CO, loss of CO is largely favoured (Scheme 4). CID spectra of [Gly–H + Zn–CO]$^+$ exhibit competitive losses of CH_2NH and H_2O. However, from the structure of **6**, it seems evident that this ion can only eliminate CH_2NH

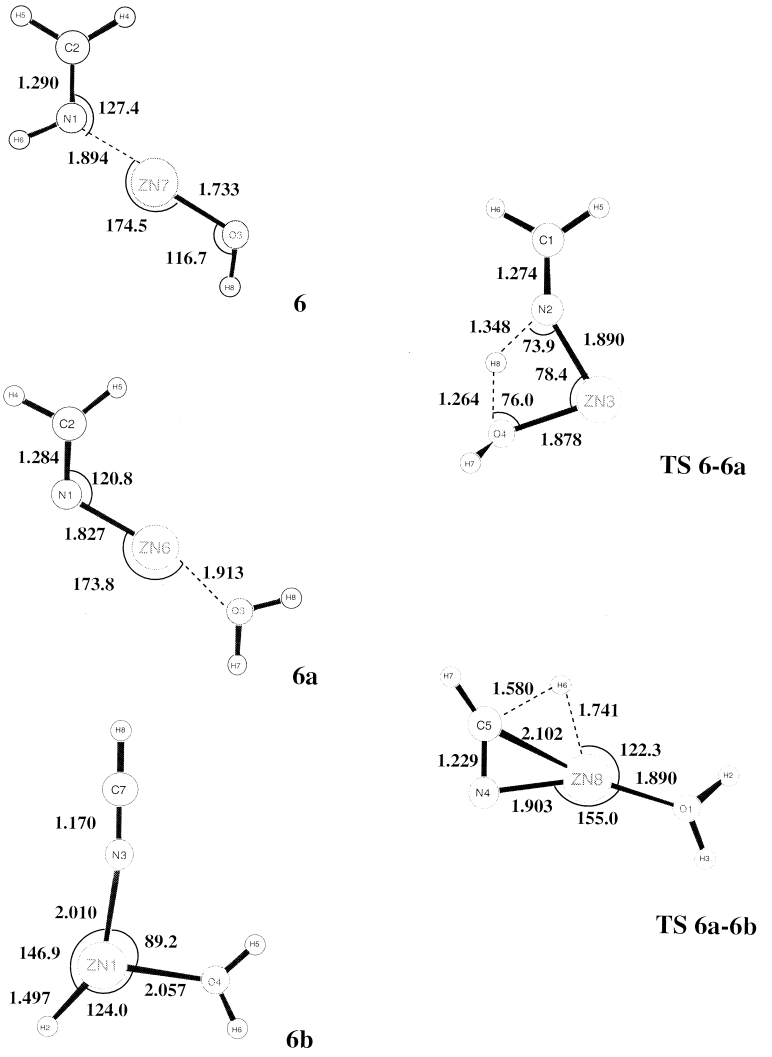

Fig. 6. Isomerization of **6** into **6a** and **6b**: geometries of **TS 6–6a**, **6a**, **TS 6a–6b** and **6b**, calculated at the MP2/basis1 level.

directly. The high endothermicity of this fragmentation from **6** (+346 kJ/mol i.e. 320 kJ/mol above **1**) is in agreement with the high energetic conditions required for its formation (see Fig. 1). In order to eliminate H_2O, a labile hydrogen must be transferred from the nitrogen to the hydroxyl oxygen.

Isomerization barriers **6–6a** and **6a–6b** (**6b** = $[HCN, ZnH, OH_2]^+$) are calculated to lie 194 and 235 kJ/mol above **1**, i.e. below the final states associated with the loss of CH_2NH from **6** and the loss of OH_2 from **6a**. Interconversion between **6**, **6a**, and **6b** are expected to occur only at higher collision energies. Moreover, the final states associated with the loss of water from **6b** are more stable than those arising from **6a**. The geometries of **6**, **6a**, **6b**, **TS 6–6a** and **TS 6a–6b** are given in Fig. 6. The H transfer from N to OH may also occur before loss of CO, generating a family of **CX** complexes. The relative energies of **CX** and of the various species associated with its decomposition are tabulated in Table 3.

Hydrogen transfer within **CX** leads to another three-ligand structure **CXA** $[CH_2NZn, OH_2, CO]^+$.

Table 3
Relative energies (in kJ/mol) associated with the various extrema describing the consecutive losses of CO and $NHCH_2$ or H_2O from the three-ligand complex **CX**

	HF/basis1	MP2/basis1	MP2/basis2// MP2/basis1
1	0	0	0
CX	−72	−51	−70
CH_2NH + $(CO\ ZnOH)^+$	160	168	131
H_2O + $(CH_2N–Zn\ CO)^+$	172	167	133
TS CX–CXA	108	88	56
CXA	23	27	20
TS CXA–CXB	198	201	137
CXB	−52	−39	−58
CO + 6	−42	−6	−26
TS 6–6a	215	240	194
6a	59	77	76
TS 6a–6b	256	289	236
6b	−35	5	17
CO,CH_2NH + $ZnOH^+$	295	345	320
H_2O,CO + $CH_2N–Zn^+$	264	277	256
H_2O + CO + $(HCNH\ Zn)^+$	215	262	215
H_2O + CO + $H–Zn–CNH^+$	123	157	134
H_2O + CO + $(HCN\ ZnH)^+$	74	106	88

The isomerization of **CX** into **CXA** may be followed by the rearrangement of **CXA** into a four-ligand isomer **CXB** $[HCN, ZnH, OH_2, CO]^+$. The geometries of species related to the isomerization of **CX** are given in Fig. 7.

The energetic barriers associated with these rearrangements are located 56 and 137 kJ/mol above **1**, respectively. **CXA** may lose either CO or H_2O or rearrange into **CXB**. Since the loss of water demands 133 kJ/mol and is observed in very low abundance in the CID spectra of $[Gly–H + Zn–CO]^+$, the isomerisation **CXA** → **CXB** is not expected. Loss of CO from **CXA**, which is the lowest energy process, leads to **6a** (76 kJ/mol above **1**). The detachment of H_2O from **6a** leads to the final state: $CH_2NZn^+ + OH_2 +$ CO at 256 kJ/mol. The rearrangment of CH_2NZn^+ into $HCN^+H\cdots Zn$ would lead to a more stable final state but the latter would lose very easily the reduced metal while this fragmentation is very minor.

In summary, the lowest energy process associated with the loss of CO from **2** requires an isomerization into a three-ligand species **CX** which can spontaneously eliminate CO to give **6**. The consecutive loss of methanimine is a high energy process. The lowest energy process associated with the consecutive losses of CO and H_2O involves (1) rearrangement of **CX** into **CXA**; (2) loss of CO from **CXA** leading to **6a** (isomeric form of **6**); (3) isomerization of **6a** into **6b**; (4) elimination of H_2O from **6b**.

*3.5. Loss of H_2O and CO from structure **B***

Structure **2** was shown to be the precursor of consecutive losses of CO and H_2O in two steps by way of the formation of $[Gly–H + Zn–CO]^+$. We propose now structure **4** to explain the formation of $[Gly–H + Zn–H_2O–CO]^+$, the intermediate ion $[Gly–H + Zn–H_2O]^+$ not being observed.

Structure **4**, a rearranged form of **2** also deprotonated on the nitrogen atom, is located 57 kJ/mol below **1**. Neither loss of H_2O nor loss of CO can occur directly from **4**. The CID spectra of $[Gly–H + Zn]^+$ show that both hydrogens involved in H_2O loss are labile. In order to eliminate such a molecule of water, the proton beared by the nitrogen atom must be shifted to the hydroxyl group. Since these two groups are initially distant, this transfer cannot directly occur from **4**. An ion **4b** in which (N)H and O(H) are located vis a vis is proposed as the appropriate intermediate (Fig. 8 and Table 4). Two pathways allow to reach **4b**, each requiring two steps. The first pathway starts with a 180 ° rotation of COOH around the C–C bond leading to **4a**. The relative energies of **TS 4–4a** and **4a** are 11 and −4 kJ/mol, respectively. Then a 180 ° rotation of HNZnH around the N–C bond leads to **4b**. This rotation requires 144 kJ/mol. In the second pathway, energetically favoured, the order of these two steps is reversed. A 180 ° rotation of HNZnH around the N–C bond gives **4a′** (−14 kJ/mol) via **TS 4–4a′** (119 kJ/mol). Then a 180 ° rotation around the C–C bond leads to **4b** and involves a transition state **TS 4a′–4b** located 15 kJ/mol above **1** (Fig. 8).

The transfer of a labile hydrogen from N to OH from **4b** leads to an ion-molecule complex **4c**. In this complex HCN is in interaction with three species:

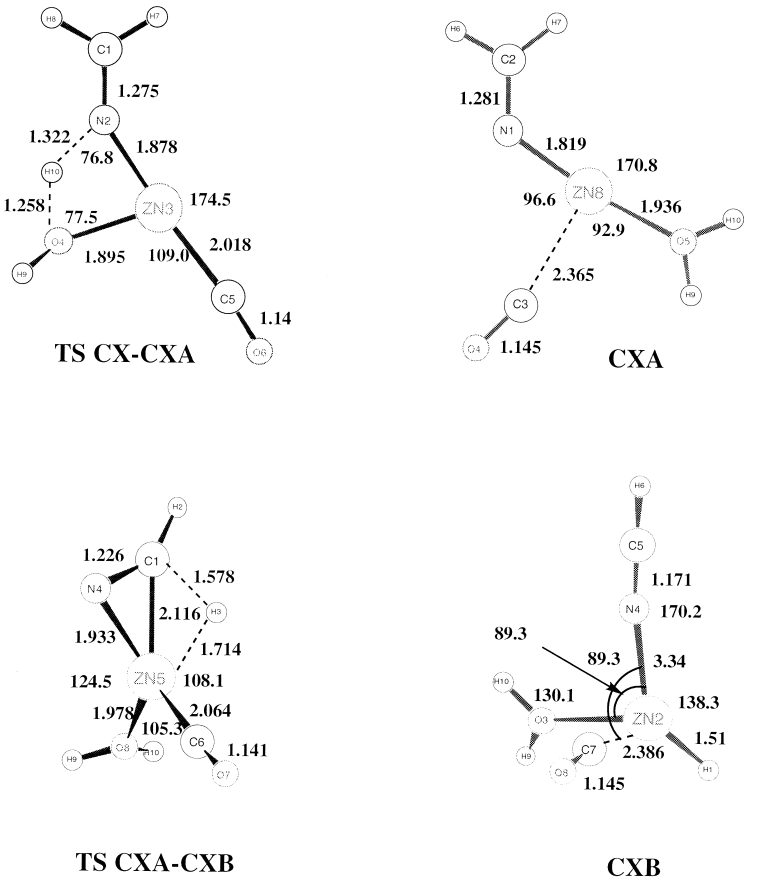

Fig. 7. Isomerization of **CX** into **CXA** and **CXB**: geometries of **TS CX–CXA**, **CXA**, **TS CXA–CXB**, and **CXB**, calculated at the MP2/basis1 level.

H_2O, CO, and ZnH^+. The transition state associated with this H migration, **TS 4b–4c**, is located 171 kJ/mol above **1**.

The geometries of **4a′**, **4b**, **TS 4–4a′**, and **TS 4a′–4b** are given in Fig. 9(a) whereas those of **4c** and **TS 4b–4c** are in Fig. 9(b).

The ion–molecule complex **4c** may either lose competitively or successively H_2O and CO, or rearrange into **4d** in which Zn^+ is ligated by H_2O, CO, H, and HCN. All final states associated with these reactions are lower in energy than **TS 4b–4c**.

4. Conclusions

In the preceding sections, the mechanisms associated with the three main collisionally induced decompositions of $[Gly–H + Zn]^+$ were described. The main results are as follows.

The elimination of CO_2 from $[Gly–H + Zn]^+$ occurs from structure **3**, a rearranged form of **1**, although this elimination would be energetically easier from **1** than from **3**; isomerization from **1** to **3** occurs before elimination of the last molecule of solvent, so that **1** is never formed.

The successive losses of H_2O and CO arise from **4**, which is formed from **3** as described previously [2].

The elimination of CO occurs from an three-ligand complex **CX**, rearranged form of **2**.

It has been demonstrated that $[Gly + CH_3OH–H + Zn]^+$ and $[Gly + Gly–H + Zn]^+$ rearrange before final evaporation of CH_3OH and Gly, respectively, leading to the formation of **3** rather than

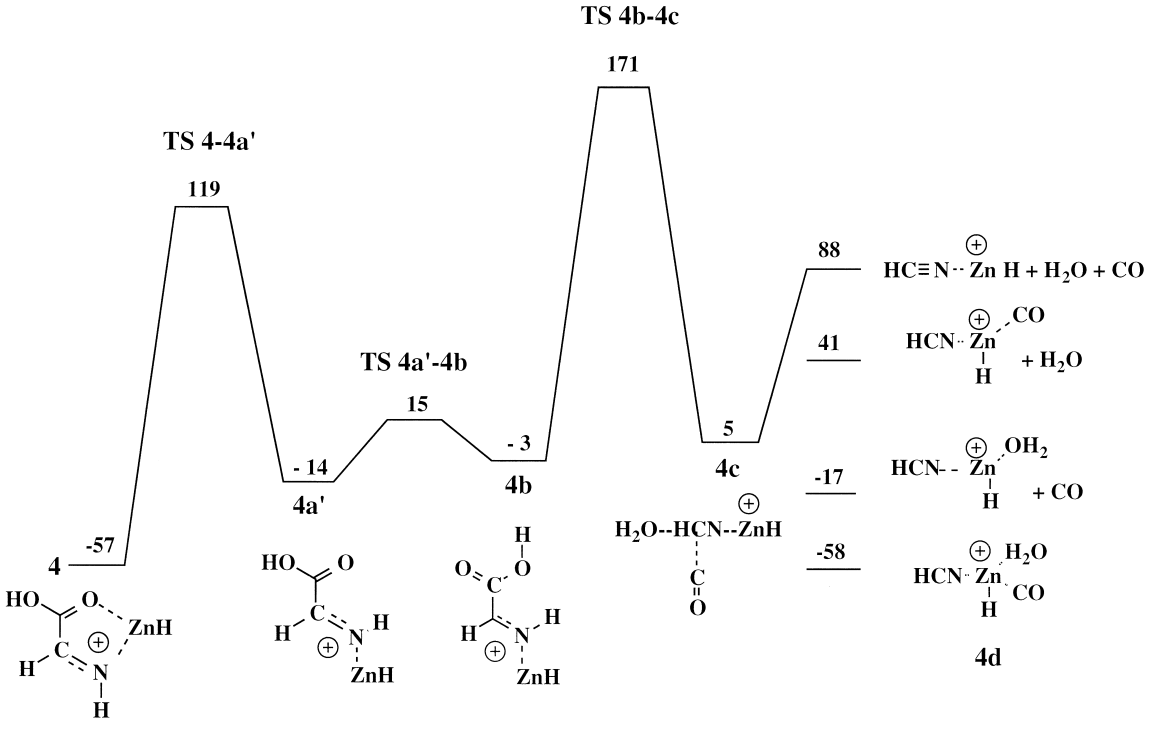

Fig. 8. Potential energy profiles associated with losses of H_2O and CO from **4**. The energy of **1** is taken as the reference.

1. The mode of formation of **2** is still unresolved. It may be hypothesized to exist in solution together with the common glycinate structure **1**, but in fact preliminary results suggest that **2** is formed, as is **3**, by way of a gas phase rearrangement within the [**1**,CH_3OH] precursor. Full details about this mechanism will be reported in a separate article.

Table 4
Relative energies (in kJ/mol) associated with the various extrema describing the consecutive losses of H_2O and CO from **4**

	MP2/basis2// MP2/basis1
4	−57
TS 4–4a′	119
4a′	−14
TS 4a′–4b	15
TS 4–4a	11
4a	−4
TS 4a–4b	144
4b	−3
TS 4b–4c	171
4c	5
4d	−58
4d–CO	−17
4d–H_2O	41
4d–H_2O–CO	88

These rearrangements are less energy demanding than the elimination of the last molecule of solvent. They have several consequences: (1) they lead to $[Gly–H + Zn]^+$ ions having different structures in solution and in the gas phase and (2) they allow Zn(II) to keep, in the molecular species $[Gly–H + Zn]^+$, more than two ligands.

The activation energies for the three primary fragmentations of $[Gly–H + Zn]^+$ are close to that calculated for the main fragmentation of protonated glycine (successive losses of H_2O and CO, 153 kJ/mol) [5]. This similarity lends support to the hope that metal cation attachment may be a viable alternative to protonation in order to generate specific fragmentations of amino acids and peptides. Work along these lines is currently underway.

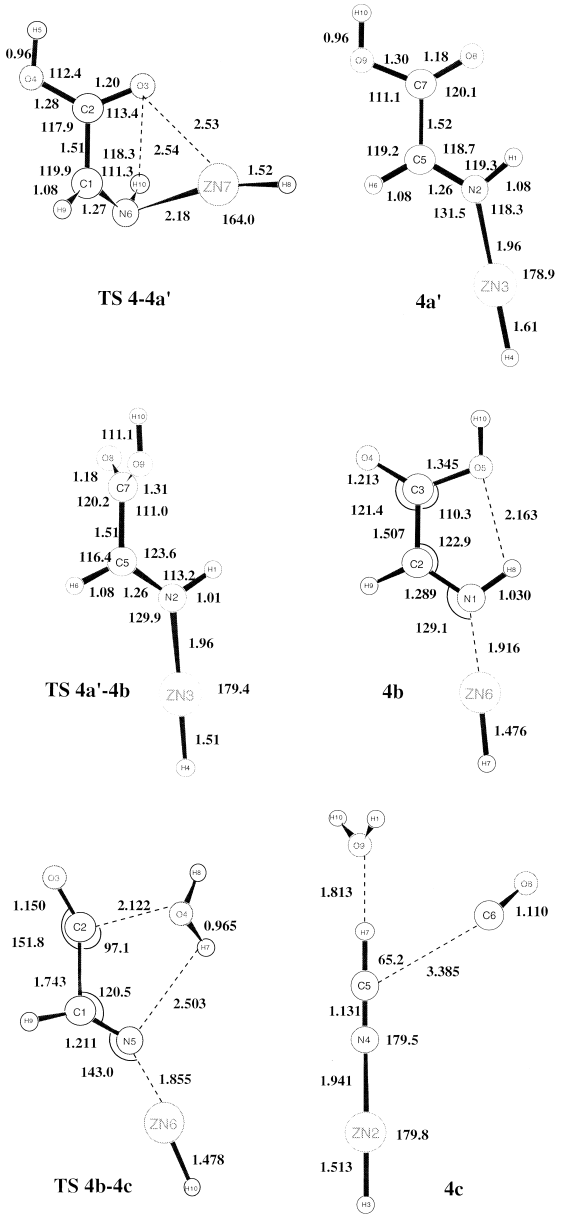

Fig. 9. Decarboxylation of **4**: geometries calculated at the MP2/basis1 level. (a) Geometries of **TS 4–4a′**; **4a′**; **TS 4a′–4b** and **4b**. (b) Geometries of **TS 4b–4c** and **4c**.

References

[1] (a) M. Dole, L.L. Mach, R.L. Hines, R.C. Mobley, L.D. Ferguson, M.B. Alice, J. Chem. Phys. 49 (1968) 2240; (b) C.M. Whitehouse, R.N. Dreyer, M. Yamashita, J.B. Fenn, Anal. Chem. 57 (1985) 675; (c) J.B. Fenn, M. Mann, C.K. Meng, S.F. Wong, C.M. Whitehouse, Mass Spectrom. Rev. 9 (1990) 37.

[2] F. Rogalewicz, Y. Hoppilliard, G. Ohanessian, Int. J. Mass Spectrom. 201 (2000) 307.

[3] (a) A.J.H. Wachters, J. Chem. Phys. 52 (1970) 1033; (b) P.J. Hay, ibid. 66 (1977) 4377; (c) G.W. Trucks, K. Raghavachari, ibid. 91 (1989) 1062.

[4] GAUSSIAN94, revision B.1, M.J. Frisch, G.W. Trucks, H.B. Schlegel, P.M.W. Gill, B.G. Johnson, M.A. Robb, J.R. Cheeseman, T.A. Keith, G.A. Petersson, J.A. Montgomery, K. Raghavachari, M.A. Al-Laham, V.G. Zakrzewski, J.V. Ortiz, J.B. Foresman, J. Cioslowski, B.B. Stefanov, A. Nanayakkara, M. Challacombe, C.Y. Peng, P.Y. Ayala, W. Chen, M.W. Wong, J.L. Andres, E.S. Replogle, R. Gomperts, R.L. Martin, D.J. Fox, J.S. Binkley, D.J. Defrees, J. Baker, J.J.P. Stewart, M. Head-Gordon, C. Gonzalez, J.A. Pople, Gaussian, Inc., Pittsburgh, PA, 1995.

[5] F. Rogalewicz, Y. Hoppilliard, Int. J. Mass Spectrom. 199 (2000) 235.